

Probing phonon-driven symmetry alterations in graphene via high-harmonic spectroscopy

Navdeep Rana¹ and Gopal Dixit^{1,*}

¹*Department of Physics, Indian Institute of Technology Bombay, Powai, Mumbai 400076 India*

(Dated: July 27, 2022)

Abstract

High-harmonic spectroscopy has become an essential ingredient in probing various ultrafast electronic processes in solids with sub-cycle temporal resolution. Despite its immense importance, sensitivity of high-harmonic spectroscopy to phonon dynamics in solids is not well known. This work addresses this critical question and demonstrates the potential of high-harmonic spectroscopy in probing intertwined phonon-electron dynamics in solids. A pump pulse excites in-plane optical phonon modes in monolayer graphene and a circularly polarised pulse is employed to probe the excited phonon dynamics that generates higher-order harmonics. We show that the coherent phonon dynamics alters the dynamical symmetry of graphene with the probe pulse and leads to the generation of symmetry-forbidden harmonics. Moreover, sidebands associated with the prominent harmonic peaks are generated as a result of the coherent dynamics. It is found that the symmetries and the characteristic timescale of the excited phonon mode determine the polarisation and positions of these sidebands. Present work opens an avenue in time-resolved probing of phonon-driven processes and dynamical symmetries in solids with sub-cycle temporal resolution.

* gdixit@phy.iitb.ac.in

I. INTRODUCTION

Vibrations of atoms within molecules and solids are fundamental processes that regulate several physical, optical and chemical properties of matter. When light triggers atomic vibrations, atoms exhibit periodic oscillations in a particular fashion and these light-induced vibrations could potentially lead to the modifications in various symmetries of solids. These modifications are dynamic in nature and result in several transient phenomena, such as light-induced superconductivity [1, 2], vibrationally-induced magnetism [3, 4], and switching of electrical polarisation [5], to name but a few. Thus, time-resolved mapping of the interplay of lattice vibration with electronic motion on electronic timescale is essential to comprehend several ubiquitous phenomena in solids, such as structural phase transition [6, 7], thermal [8, 9] and optical properties [10–12]; and predicting new concepts in solids. Several spectroscopy and imaging-based methods are employed to probe lattice vibrations in solids [13–20]. However, probing transiently-evolving intertwined lattice-electronic dynamics and dynamical symmetries of solids in the presence of light in a single experimental setup are challenging. Present work addresses this crucial problem.

High-harmonic generation (HHG) is a non-perturbative nonlinear frequency up-conversion process and is sensitive to the sub-cycle electron dynamics driven by intense laser. Over the last decade, high-harmonic spectroscopy became an emerging method to interrogate various equilibrium and non-equilibrium properties of solids by investigating the emitted spectrum during HHG [21–35]. In spite of the tremendous applications of high-harmonic spectroscopy, impact of lattice vibration on HHG from solids remains uncharted territory, except recent work [36, 37]. Present work focuses to highlight the abilities of high-harmonic spectroscopy in time-resolved mapping of the interplay of coherent lattice vibrations and electronic motions; and transiently-evolving symmetries of solids during the dynamics.

In the following, we will demonstrate that the high-harmonic spectroscopy of the coherent lattice dynamics leads to the generations of the higher-order sidebands along with the main harmonic peaks in the high-harmonic spectrum. The frequency and symmetry of the coherently excited phonon mode are imprinted in the position and polarisation of the sidebands, respectively. Moreover, symmetry-forbidden harmonics are allowed due to the symmetry alterations caused by the coherent lattice dynamics.

To illustrates the sensitivity of the coherent phonon dynamics to high-harmonic spec-

troscopy, two-dimensional graphene with \mathbf{D}_{6h} point group symmetry is chosen. The phonon spectrum of graphene is consist of three acoustic and three optical phonon branches. Out of the three optical phonon modes, one phonon mode is out-of-plane where the vibrations are out of the two-dimensional plane of graphene, and other two are in-plane modes in which lattice vibrations are confined within the plane of graphene [38]. In-plane optical phonon modes are considered in this work. At the Γ point, there are two degenerate in-plane optical modes with phonon frequency of 194 meV, which corresponds to phonon oscillation period of ~ 21 femtoseconds [38]. These phonon modes are represented as E_{2g} or G modes and are Raman active. It is known that light can couple to a phonon mode at the Brillouin zone centre and therefore E_{2g} Raman-active mode can be excited by stimulated Raman excitation either via a broad pulse that covers a bandwidth of 194 meV or via using two laser pulses with a difference of 194 meV in photon energy. By tuning the polarisation of the phonon exciting pulse either along $\Gamma - K$ or $\Gamma - M$ direction, one of the two in-plane phonon modes can be excited selectively.

II. COMPUTATIONAL METHODS

To incorporate coherent phonon dynamics, nearest-neighbour tight-binding Hamiltonian is extended from static to time domain as

$$\hat{\mathcal{H}}_{\mathbf{k}}(t) = -\gamma(t) \sum_{i \in nn} e^{i\mathbf{k} \cdot \mathbf{d}_i(t)} \hat{a}_{\mathbf{k}}^\dagger \hat{b}_{\mathbf{k}} + \text{H. c.} \quad (1)$$

Here, $\gamma(t) = \gamma_0 e^{-(|\mathbf{d}_i(t)|-a)/\delta}$ is the time-dependent nearest-neighbour hopping energy, which is modelled to capture the temporal variations in the relative distance between nearest-neighbour atoms ($\mathbf{d}_i = a = 1.42 \text{ \AA}$) [39]. $\gamma_0 = 2.7 \text{ eV}$ is the nearest-neighbour hopping energy and $\delta = 0.184a_0$ is the width of the decay function with $a_0 = 2.46 \text{ \AA}$ as the lattice parameter of the equilibrium structure [40].

Semiconductor-Bloch equations corresponding to time-dependent Hamiltonian given in Eq. (1) are solved as

$$\frac{d}{dt} \rho_{cv}^{\mathbf{k}} = \left[-i\varepsilon_{cv}(\mathbf{k}_t, t) + \frac{1}{T_2} \right] \rho_{cv}^{\mathbf{k}} + i\mathbf{E}(t) \cdot \mathbf{d}_{cv}(\mathbf{k}_t, t) [\rho_{vv}^{\mathbf{k}} - \rho_{cc}^{\mathbf{k}}] \quad \text{and} \quad (2a)$$

$$\frac{d}{dt} \rho_{vv}^{\mathbf{k}} = i\mathbf{E}(t) \cdot \mathbf{d}_{vc}(\mathbf{k}_t, t) \rho_{cv}^{\mathbf{k}} + \text{c.c.} \quad (2b)$$

Here, the vector potential and the electric field corresponding to the driving laser field are represented as $\mathbf{A}(t)$ and $\mathbf{E}(t)$, respectively, and are related as $\mathbf{E}(t) = -d\mathbf{A}(t)/dt$. $\mathbf{d}_{cv}(\mathbf{k})$ and $\varepsilon_{cv}(\mathbf{k})$ are, respectively, the dipole matrix elements and the band-gap energy between conduction and valence bands at given \mathbf{k} with $\mathbf{d}_{cv}(\mathbf{k}) = i\langle c, \mathbf{k} | \nabla_{\mathbf{k}} | v, \mathbf{k} \rangle$. The matrix elements become time-dependent due to coherent phonon dynamics and are updated smoothly at each consecutive time-steps during the phonon dynamics. To account the interband decoherence, a phenomenological term with a constant dephasing time T_2 is introduced. Here, $\mathbf{k}_t = \mathbf{k} + \mathbf{A}(t)$.

High-harmonic spectrum is calculated as

$$\mathcal{I}(\omega) = \left| \mathcal{FT} \left(\frac{d}{dt} \mathbf{J}(t) \right) \right|^2, \quad (3)$$

where \mathcal{FT} stands for the Fourier transform. The total current $\mathbf{J}(t)$ is calculated by integrating $\mathbf{J}(\mathbf{k}, t)$ over the entire Brillouin zone as

$$\mathbf{J}(\mathbf{k}, t) = \sum_{m,n \in \{c,v\}} \rho_{mn}^{\mathbf{k}}(t) \mathbf{p}_{nm}(\mathbf{k}_t, t), \quad (4)$$

where $\mathbf{p}_{nm}(\mathbf{k}) = \langle n, \mathbf{k} | \nabla_{\mathbf{k}} \hat{\mathcal{H}}_{\mathbf{k}} | m, \mathbf{k} \rangle$ is momentum matrix-element. We have adopted the same methodology for HHG from a solid with phonon dynamics as given in our earlier work [41]. The ellipticity and the phases of harmonics are estimated by following the recipe given in Ref. [42].

It is assumed that a pump-pulse initiate the coherent excitation of an in-plane Raman active phonon mode in graphene. The excited phonon mode is probed by the high-harmonic generating pulse. The excitation of the phonon mode is approximated by direct initiation of the coherent vibrations of carbon atoms within adiabatic approximation. Circularly-polarised pulse with a wavelength of 2.0 μm and peak intensity of 1×10^{11} W/cm^2 is used to generate high-harmonics in graphene with and without coherent phonon dynamics. The pulse duration is 100 fs, which is much longer than an oscillation period of in-plane phonon dynamics $\simeq 21$ fs. Moreover, the coherence times of these phonon modes of around 1 ps are reported [43, 44]. Parameters of the harmonic generating laser are similar to the ones used earlier for probing electron dynamics in graphene [45, 46].

III. RESULTS AND DISCUSSION

High-harmonic spectrum corresponding to monolayer graphene without phonon dynamics is presented in Fig. 1(a). We have employed left-handed circularly polarised laser pulse for HHG in graphene with and without phonon dynamics. As dictated by the symmetry constraints and selections rules, it is expected that circularly polarised pulse yields $(6m \pm 1)$ -orders of harmonics from an inversion-symmetric graphene with the six-fold symmetry [47, 48]. Here, $m = 0, 1, 2, \dots$ is a positive integer. In this case, third harmonic is symmetry forbidden. On the other hand, linearly polarised laser pulse leads to $(2m + 1)$ -orders of harmonics as shown earlier [49]. Our results shown in Fig. 1(a) are consistent with the selection rules and earlier report [47, 48]. Graphene is not chiral in nature, so left- and right-handed circular laser pulses yield same harmonic spectra.

After discussing HHG from graphene without phonon dynamics, let us investigate how the in-plane phonon modes affect the harmonic spectrum shown in Fig. 1(a). For this purpose, we coherently excite one of the two degenerate in-plane phonon modes and assume that the excitation is done prior to the probe harmonic pulse. Figure 1(b) presents the harmonic spectrum corresponding to coherently excited longitudinal optical (iLO) phonon mode. The spectrum in Fig. 1(b) is drastically different from the one without phonon dynamics [see Fig. 1(a)]. There are only odd harmonics in the spectrum as the iLO phonon mode preserves the inversion symmetry in graphene [41]. Moreover, the spectrum exhibits multiple sidebands along with the main odd harmonics as evident from Fig. 1(b). The coherent excitation of the in-plane transverse optical (iTO) phonon mode also leads to multiple sidebands along with the odd harmonics as visible from Fig. 1(c). In both cases, the energy separation between the successive sidebands is equal to the energy of the excited phonon (iLO or iTO) mode, i.e., 194 meV. Therefore, the energy of the excited phonon mode is encoded in the spectra. Apparently, it seems that the spectra is insensitive to the symmetry of the excited phonon mode as both iLO and iTO phonon modes yields similar harmonic spectra [see Figs. 1(b) and 1(c)]. In the following, we will show that this is not the case and the symmetry of the excited phonon mode is encoded in the polarisation properties of the spectra.

Not only coherent phonon dynamics leads to the generation of the multiple sidebands but also the forbidden harmonics become allowed. As stated earlier, third harmonic is

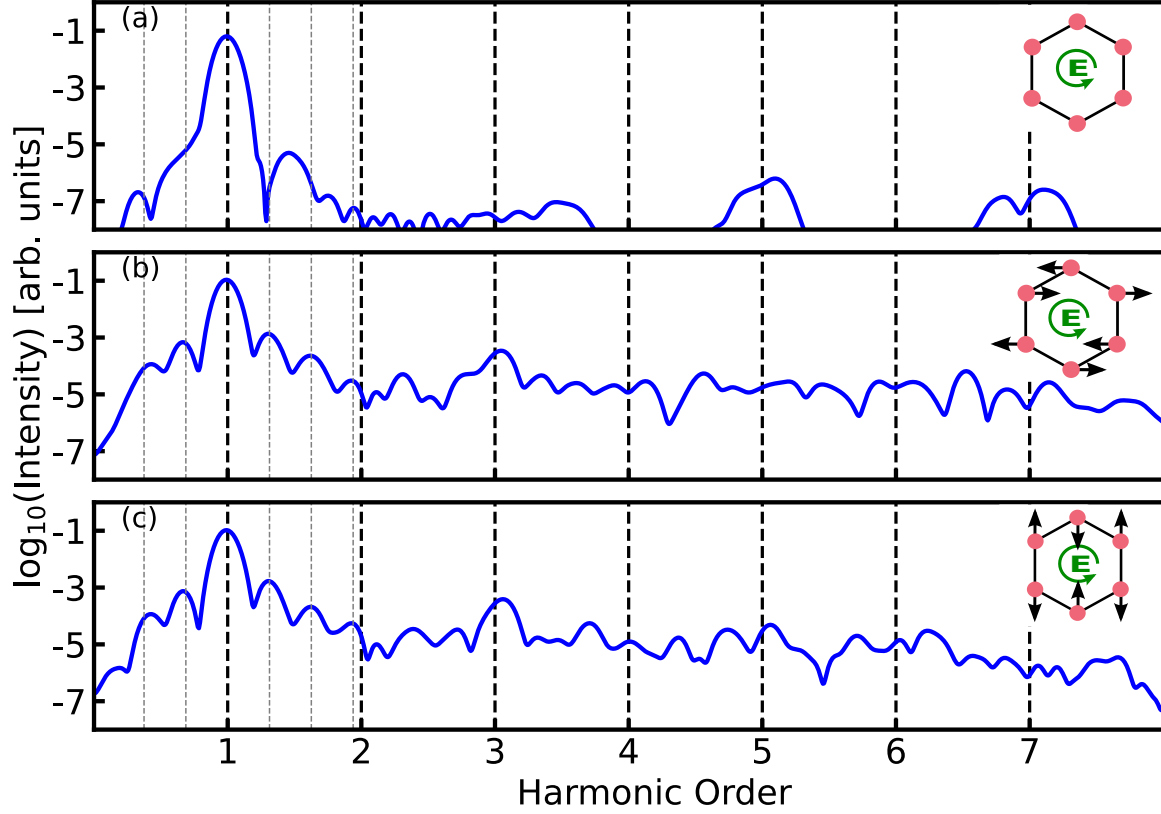


FIG. 1. High-harmonic spectra, generated by left-handed circularly polarised laser pulse, of two-dimensional graphene with and without coherent phonon dynamics. (a) The spectra of the graphene without phonon dynamics. The spectra of graphene with the coherent in-plane (b) longitudinal optical (iLO) phonon mode and (c) transverse optical (iTO) phonon mode. In all the spectra, sidebands corresponding to the prominent harmonic peaks are identified at frequencies $(\omega_0 \pm n\omega_{\text{ph}})$ with ω_{ph} as the phonon frequency, ω_0 as the frequency of the probe laser pulse and n is an integer. The unit cell of the graphene with the eigenvector of a particular phonon mode and polarisation of the harmonic generating probe pulse are shown in the respective insets. Results are presented for $T_2 = 10$ fs and a maximum $0.03a_0$ displacement of atoms from their equilibrium positions during coherent phonon dynamics where a_0 is the lattice parameter of the equilibrium structure. Our findings remain qualitatively same for T_2 ranging from 5 to 30 fs and for displacements ranging from $0.01a_0$ to $0.05a_0$ with respect to the equilibrium positions of the carbon atoms.

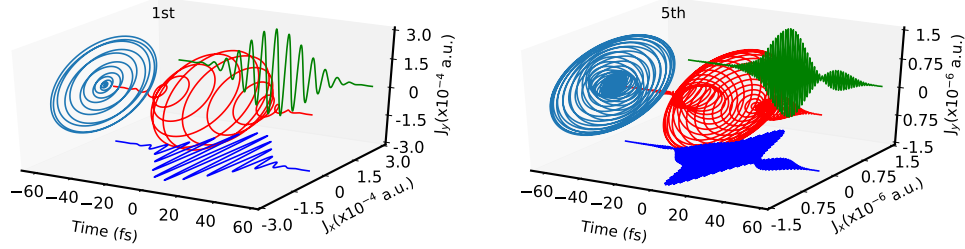


FIG. 2. Lissajous figure (in cyan), total (in red), x (in blue) and y (in green) components of the first and the fifth harmonics in time-domain corresponding to the spectrum shown in Fig. 1(a) for graphene without phonon dynamics.

absent for the circular laser driven HHG from graphene without phonon [see Fig. 1(a)]. However, dynamics of the coherent E_{2g} phonon mode reduces graphene's six-fold symmetry into two-fold dynamically, which allows the generation of $(2m \pm 1)$ harmonic orders. The presence of the third harmonic in both cases, graphene with (iLO or iTO) phonon mode, is a signature of the symmetry reduction as evident from Fig. 1(b) and 1(c). At a glance, it seems that the criteria for HHG is same for linearly polarised laser pulse [$(2m + 1)$ orders and third harmonic] and the combination of the phonon-driven symmetry reduction with circularly polarised laser pulse [$(2m \pm 1)$ orders and third harmonic]. To distinguish the two situations, let us analyse the polarisation properties of the emitted harmonics.

Figure 2 displays the time-domain representations of the x and y components of the first and fifth harmonics of the spectrum in Fig. 1(a). It is known that the polarisation of a given harmonic for a material with l -fold symmetry is determined by $lm + \sigma$, where $\sigma = +(-)1$ represents the m^{th} harmonic's polarisation, which is same (opposite) as the helicity of the driving laser pulse [47]. It is straightforward to see that $(lm - 1)^{\text{th}}$ and $(lm + 1)^{\text{th}}$ harmonics are circularly polarised with $\sigma = -1$ and $\sigma = 1$, respectively. In present case, the first and fifth harmonics are circularly polarised with opposite helicity and is consistent with earlier findings [48, 50].

As stated above, $(2m \pm 1)$ harmonic orders are allowed due to phonon-driven dynamical symmetry reduction from six-fold to two-fold, which leads to the generation of the third harmonic. Moreover, this dynamical symmetry reduction also alters the polarisation properties of the emitted harmonics. The x and y components of the first, third, and fifth harmonics in

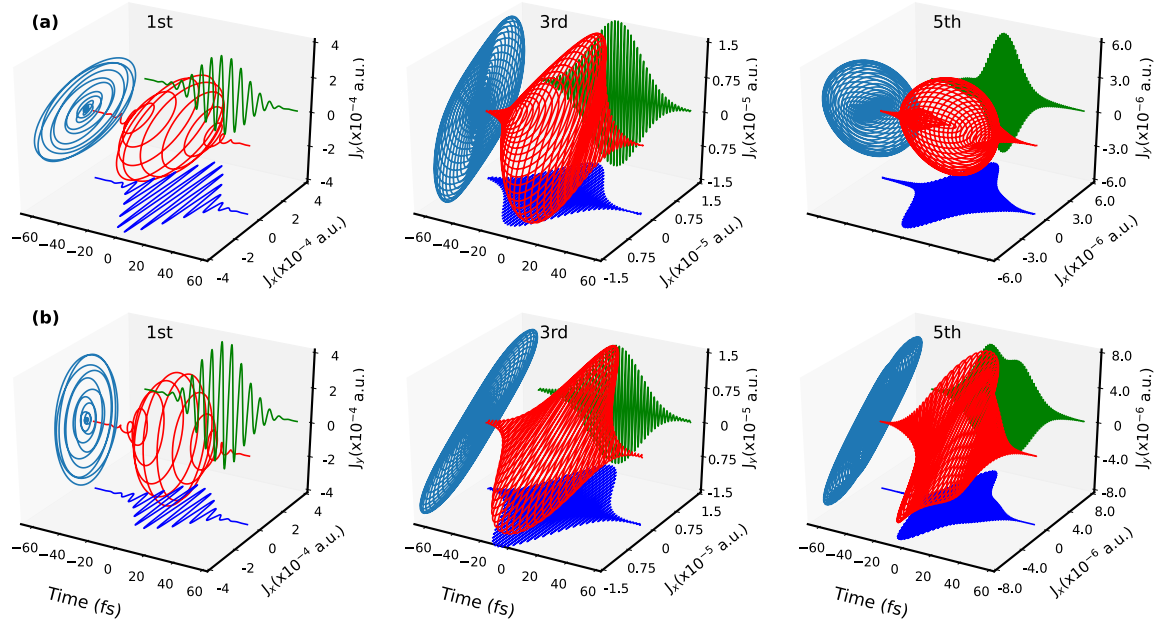


FIG. 3. Same as Fig. 2 for the first, third and fifth harmonics in time-domain for graphene with (a) iLO and (b) iT0 phonon modes. In the case of iLO (iT0) phonon mode, the ellipticities of the first, third and fifth harmonics are 0.63 (0.62), 0.77 (0.79), and 0.93 (0.96), respectively. Also, the phase differences between x and y components of the first, third and fifth harmonics are 90° (90°), 40° (35°), and 125° (45°), respectively.

time domain for graphene with iLO and iT0 phonon modes are presented in Figs. 3(a) and 3(b), respectively. As evident from the figure, the ellipticity of the first harmonic reduces drastically from 1 for graphene without phonon to 0.63 for graphene with phonon. The change in the ellipticity can be understood as follow: When iLO phonon mode is excited, carbon atoms vibrate along the X direction, which increases the velocity of the electrons in the X direction. It is known that the intraband current is proportional to the velocity, and low-order harmonics in graphene are dominated by the intraband current [49, 51]. Thus, the major axis of the ellipse is along the X direction in the case of the first harmonic, which reduces the ellipticity from 1 to 0.63.

Similarly, the excitation of the iT0 mode leads the vibrations of the atoms along Y direction. This provides an additional velocity component to electrons in the Y direction,

which translate to the major axis of the ellipse along the Y direction. The ellipticity of the fifth harmonic, corresponding to graphene without phonon to with iLO (iTO) phonon mode, changes significantly, i.e., from 1 to 0.93 (0.96). Not only the phonon dynamics modifies the ellipticity of the harmonics significantly but also changes the phase between the x and y components of the harmonics. In the case of iLO (iTO) mode, the phase differences between the components for first and fifth harmonics are 90° (90°) and 125° (45°), respectively (see Fig. 3). The ellipticity and the phase difference of the third harmonic for graphene with iLO (iTO) mode is 0.77 (0.79), and 40° (35°), respectively. Thus, the changes in the ellipticity and phase indicate that the harmonics are sensitive to the symmetry of the excited phonon mode as reflected from Fig. 3.

After demonstrating how the information of the excited phonon mode and its symmetry are imprinted in the main harmonics and their polarisation properties, let us analyse what informations are encoded in the sidebands associated with prominent harmonics. Time-domain picture of the x and y components of the first, second and third sidebands corresponding to the first harmonic corresponding to graphene with iLO phonon mode is shown in Fig. 4(a). All three sidebands have nonzero x and y components as evident from the figure. The same is true for the sidebands associated with iTO phonon excitation as reflected from Fig. 4(b). Moreover, the ellipticities of the first, second and third sidebands of the first harmonic corresponding to graphene with iLO (iTO) phonon mode read as 0.98 (0.56), 0.72 (0.95), and 0.59 (0.67), respectively. Also, the phases between the x and y components of the first, second and third sidebands of the iLO (iTO) mode are 85° (90°), 70° (135°), and 60° (75°), respectively. Thus, the analysis of Fig. 4 establishes that the polarisation and the phase properties of the sidebands are different for different phonon mode. However, it is not obvious why the sidebands have nonzero x and y components, whereas a particular phonon mode (iLO or iTO) induces atomic vibrations along a particular direction (X or Y).

To know the origin of the nonzero x and y components of the sidebands, we employ Floquet formalism to graphene with coherently excited phonon mode and circularly polarised probe pulse. Floquet formalism determines dynamical (spatio-temporal) symmetries (DSs) of the system, which dictate selection rules for the sidebands. The n^{th} -order sideband obeys the symmetry constraint as $\hat{X}^t \mathbf{E}_{s,n}(t) [\hat{X}^t \mathbf{E}(t)]^\dagger = \mathbf{E}_{s,n} \mathbf{E}^\dagger(t)$ with the condition that the spatial symmetries of \hat{X}^t and the probe pulse are same [52]. Here, \hat{X}^t is a DS, and the electric fields associated with n^{th} -order sideband and the probe laser are represented by

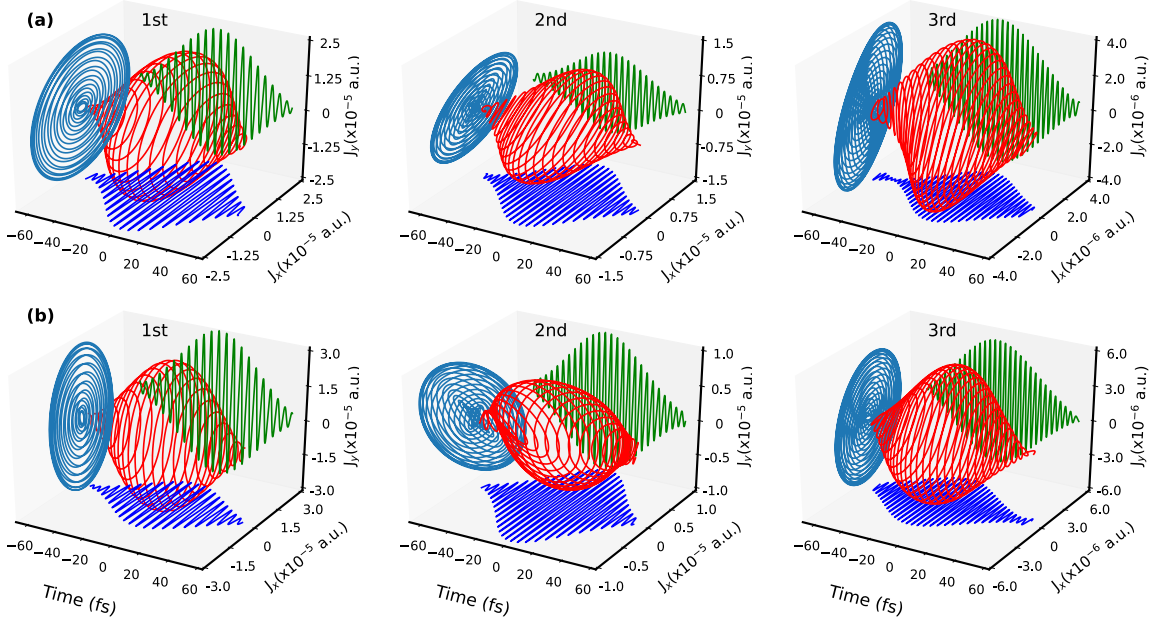


FIG. 4. Same as Fig. 2 for the first, second and third sidebands in time-domain associated with the first harmonic for graphene with (a) iLO phonon mode corresponding to Fig. 1(b), and (b) iTO phonon mode corresponding to Fig. 1(c). The ellipticities of the first, second and third sidebands corresponding to iLO (iTO) phonon mode are 0.98 (0.56), 0.72 (0.95), and 0.59 (0.67), respectively. The phase differences between x and y components of the first, second and third sidebands corresponding to iLO (iTO) phonon mode are 85° (90°), 70° (135°), and 60° (75°), respectively.

$\mathbf{E}_{s,n}(t)$ and $\mathbf{E}(t)$, respectively. The Raman tensor, denoted as $\mathcal{R}_n(t) = \mathbf{E}_{s,n}(t)\mathbf{E}(t)^\dagger$, has to be invariance under the operation of the DSs [52]. In the following, we will follow the same treatment as given in Refs. [41, 52] to investigate the properties of the sidebands using DSs within Floquet formalism.

In the present case, $\mathcal{D}_1 = \hat{\sigma}_y \cdot \mathcal{T}$ is the DS, which leaves the system with iLO phonon mode invariant. Here, $\hat{\sigma}_y$ is the reflection with respect to y -axis, and $\hat{\mathcal{T}}$ is the time-reversal operator. Thus, the condition associated with the sidebands is determined as $\hat{\mathcal{D}}_1 \mathcal{R}_n(t) =$

$\mathcal{R}_n(t)$ with

$$\mathcal{R}_n(t) = \mathbf{E}_{s,n}(t)\mathbf{E}(t)^\dagger = \begin{bmatrix} E_{s,n_x}E_x^* & E_{s,n_x}E_y^* \\ E_{s,n_y}E_x^* & E_{s,n_y}E_y^* \end{bmatrix}. \quad (5)$$

Let us substitute the expression of $\mathbf{E}^\dagger(t) = [\cos(\omega_0 t)E_x^\dagger \quad \sin(\omega_0 t)E_y^\dagger]$ with ω_0 is the frequency of the probe pulse in the above equation, the expression of the Raman tensor reads as

$$\mathcal{R}_n(t) = \sin[(n\omega_{\text{ph}} + \omega_0)t] \begin{bmatrix} \cos(\omega_0 t)E_{s,n_x} \\ \sin(\omega_0 t)E_{s,n_y} \end{bmatrix}. \quad (6)$$

Here, ω_{ph} is the frequency of the phonon mode. On operating \mathcal{D}_1 on $\mathcal{R}_n(t)$ leads the following expression of the invariant $\mathcal{R}_n(t)$ as

$$\sin[(m\omega_{\text{ph}} + \omega_0)t] \begin{bmatrix} \cos(\omega_0 t)E_{s,n_x} \\ \sin(\omega_0 t)E_{s,n_y} \end{bmatrix} = \sin[-(n\omega_{\text{ph}} + \omega_0)t] \begin{bmatrix} -\cos(\omega_0 t)E_{s,n_x} \\ -\sin(\omega_0 t)E_{s,n_y} \end{bmatrix}. \quad (7)$$

Now it is straightforward to notice that all the sidebands exhibit nonzero x and y components. The ellipticity and the phase difference are estimated from the nonzero components and our numerical results shown in Fig. 4 are consistent with the present analysis. If linearly polarised probe pulse is used instead of the circularly polarised pulse, the odd- and even-order sidebands are, respectively, polarised perpendicular and parallel to the polarisation of probe pulse in the case of graphene with iLO phonon mode. On the other hand, iTO phonon mode leads all sidebands polarised along the direction of the probe pulse [41].

Our findings are drastically different from the recent reported work where HHG is employed to probe phonon dynamics in hexagonal boron nitride (h-BN). In Ref. [36], it has been reported that the phonon dynamics leads the generation of the forbidden second harmonic and enhancement of the third harmonic in few-layer h-BN. Moreover, coherent phonon in h-BN leads to the attenuation of the harmonic spectrum with no discrete harmonics [37]. HHG becomes sensitive to the carrier-envelope phase of the probe pulse when the pulse duration and the period of the excited phonon are similar [37].

IV. CONCLUSION

In conclusion, we have explored the potential of high-harmonic spectroscopy in probing intertwined coherent-phonon electron dynamics in solids. To this end, coherent excitation of

both in-plane iLO and iTO Raman-active phonon modes in graphene are considered. The six-fold symmetry of the graphene reduces to two-fold dynamically due to the coherent phonon excitation. As a result of this symmetry alteration, symmetry-forbidden third harmonic of circularly polarised probe pulse is generated. Moreover, coherent phonon leads to the generation of the sidebands corresponding to the prominent harmonic peaks. Floquet formalism of the dynamical symmetries of the system is applied to understand the properties of the sidebands. It is found that the positions of the sidebands are determined by the energy of the excited phonon modes. Moreover, the dynamical symmetries of the system, consists of graphene with an excited phonon mode and probe pulse, determine the polarisation of the sidebands. Thus, polarisation properties of the sidebands are a sensitive probe of the dynamical symmetries. Present study could be extended to bilayer graphene where infrared-active phonon modes can be expressed in terms of double degenerate in-plane Raman-active phonon modes of monolayer graphene [53, 54]. Moreover, this work provides a platform to study non-linear phononics with sub-cycle temporal resolution.

ACKNOWLEDGEMENTS

We acknowledge fruitful discussion with M S Mrudul (Uppsala University), and Klaus Reimann (MBI Berlin). G. D. acknowledges support from Science and Engineering Research Board (SERB) India (Project No. MTR/2021/000138).

-
- [1] W. Hu, S. Kaiser, D. Nicoletti, C. R. Hunt, I. Gierz, M. C. Hoffmann, M. Le Tacon, T. Loew, B. Keimer, and A. Cavalleri, *Nature Materials* **13**, 705 (2014).
 - [2] M. Mitrano, A. Cantaluppi, D. Nicoletti, S. Kaiser, A. Perucchi, S. Lupi, P. Di Pietro, D. Pontiroli, M. Riccò, S. R. Clark, D. Jaksch, and A. Cavalleri, *Nature* **530**, 461 (2016).
 - [3] M. Rini, R. Tobey, N. Dean, J. Itatani, Y. Tomioka, Y. Tokura, R. W. Schoenlein, and A. Cavalleri, *Nature* **449**, 72 (2007).
 - [4] T. F. Nova, A. Cartella, A. Cantaluppi, M. Först, D. Bossini, R. V. Mikhaylovskiy, A. V. Kimel, R. Merlin, and A. Cavalleri, *Nature Physics* **13**, 132 (2017).

- [5] R. Mankowsky, A. von Hoegen, M. Först, and A. Cavalleri, *Physical Review Letters* **118**, 197601 (2017).
- [6] D. Bansal, J. L. Niedziela, S. Calder, T. Lanigan-Atkins, R. Rawl, A. H. Said, D. L. Abernathy, A. I. Kolesnikov, H. Zhou, and O. Delaire, *Nature Physics* **16**, 669 (2020).
- [7] M. Hase, P. Fons, K. Mitrofanov, A. V. Kolobov, and J. Tominaga, *Nature communications* **6**, 1 (2015).
- [8] J. Niedziela, D. Bansal, A. May, J. Ding, T.L.-Atkins, G. Ehlers, D. Abernathy, A. Said, and O. Delaire, *Nature Physics* **15**, 73 (2019).
- [9] D. Bansal, J. Niedziela, R. Sinclair, V. Garlea, D. Abernathy, S. Chi, Y. Ren, H. Zhou, and O. Delaire, *Nature Communications* **9**, 15 (2018).
- [10] H. Katsuki, J. Delagnes, K. Hosaka, K. Ishioka, H. Chiba, E. Zijlstra, M. Garcia, H. Takahashi, K. Watanabe, M. Kitajima, Y. Matsumoto, K. G. Nakamura, and K. Ohmori, *Nature communications* **4**, 1 (2013).
- [11] B. Fultz, *Progress in Materials Science* **55**, 247 (2010).
- [12] A. Gambetta, C. Manzoni, E. Menna, M. Meneghetti, G. Cerullo, G. Lanzani, S. Tretiak, A. Piryatinski, A. Saxena, R. Martin, and A. Bishop, *Nature Physics* **2**, 515 (2006).
- [13] L. Dhar, J. A. Rogers, and K. A. Nelson, *Chemical Reviews* **94**, 157 (1994).
- [14] T. Debnath, D. Sarker, H. Huang, Z.-K. Han, A. Dey, L. Polavarapu, S. V. Levchenko, and J. Feldmann, *Nature communications* **12**, 1 (2021).
- [15] D. Graf, F. Molitor, K. Ensslin, C. Stampfer, A. Jungen, C. Hierold, and L. Wirtz, *Nano Letters* **7**, 238 (2007).
- [16] A. Virga, C. Ferrante, G. Batignani, D. De Fazio, A. Nunn, A. Ferrari, G. Cerullo, and T. Scopigno, *Nature Communications* **10**, 1 (2019).
- [17] J. Koivistoinen, P. Myllyperkio, and M. Pettersson, *Journal of Physical Chemistry Letters* **8**, 4108 (2017).
- [18] N. Rana, A. P. Roy, D. Bansal, and G. Dixit, *npj Computational Materials* **7**, 1 (2021).
- [19] S. B. Brown, A. Gleason, E. Galtier, A. Higginbotham, B. Arnold, A. Fry, E. Granados, A. Hashim, C. G. Schroer, A. Schropp, F. Seiboth, F. Tavella, Z. Xing, W. Mao, H. Lee, and B. Nagler, *Science advances* **5**, eaau8044 (2019).
- [20] D. J. Flannigan, *Physics* **11**, 53 (2018).

- [21] T. T. Luu, M. Garg, S. Y. Kruchinin, A. Moulet, M. T. Hassan, and E. Goulielmakis, *Nature* **521**, 498 (2015).
- [22] O. Schubert, M. Hohenleutner, F. Langer, B. Urbanek, C. Lange, U. Huttner, D. Golde, T. Meier, M. Kira, S. W. Koch, and R. Huber, *Nature Photonics* **8**, 119 (2014).
- [23] M. Mrudul, Á. Jiménez-Galán, M. Ivanov, and G. Dixit, *Optica* **8**, 422 (2021).
- [24] M. S. Mrudul and G. Dixit, *Journal of Physics B* **54**, 224001 (2021).
- [25] M. Hohenleutner, F. Langer, O. Schubert, M. Knorr, U. Huttner, S. W. Koch, M. Kira, and R. Huber, *Nature* **523**, 572 (2015).
- [26] B. Zaks, R.-B. Liu, and M. S. Sherwin, *Nature* **483**, 580 (2012).
- [27] A. Pattanayak, M. S. Mrudul, and G. Dixit, *Physical Review A* **101**, 013404 (2020).
- [28] F. Langer, C. P. Schmid, S. Schlauderer, M. Gmitra, J. Fabian, P. Nagler, C. Schüller, T. Korn, P. Hawkins, J. Steiner, U. Huttner, S. Koch, M. Kira, and R. Huber, *Nature* **557**, 76 (2018).
- [29] M. S. Mrudul, N. Tancogne-Dejean, A. Rubio, and G. Dixit, *npj Computational Materials* **6**, 1 (2020).
- [30] T. T. Luu and H. J. Wörner, *Nature Communications* **9**, 1 (2018).
- [31] H. B. Banks, Q. Wu, D. C. Valocin, S. Mack, A. C. Gossard, L. Pfeiffer, R.-B. Liu, and M. S. Sherwin, *Physical Review X* **7**, 041042 (2017).
- [32] M. S. Mrudul, A. Pattanayak, M. Ivanov, and G. Dixit, *Physical Review A* **100**, 043420 (2019).
- [33] Y. Bai, F. Fei, S. Wang, N. Li, X. Li, F. Song, R. Li, Z. Xu, and P. Liu, *Nature Physics* , 1 (2020).
- [34] S. Imai, A. Ono, and S. Ishihara, *Physical Review Letters* **124**, 157404 (2020).
- [35] M. Borsch, C. P. Schmid, L. Weigl, S. Schlauderer, N. Hofmann, C. Lange, J. T. Steiner, S. W. Koch, R. Huber, and M. Kira, *Science* **370**, 1204 (2020).
- [36] J. S. Ginsberg, M. M. Jadidi, J. Zhang, C. Y. Chen, S. H. Chae, G. N. Patwardhan, L. Xian, N. Tancogne-Dejean, K. Watanabe, T. Taniguchi, J. Hone, A. Rubio, and A. Gaeta, arXiv preprint arXiv:2107.11959 (2021).
- [37] O. Neufeld, J. Zhang, U. De Giovannini, H. Hubener, and A. Rubio, arXiv preprint arXiv:2203.05033 (2022).
- [38] J.-H. Kim, A. Nugraha, L. Booshehri, E. Hároz, K. Sato, G. Sanders, K.-J. Yee, Y.-S. Lim, C. Stanton, R. Saito, and J. Kono, *Chemical Physics* **413**, 55 (2013).

- [39] V. Mohanty and E. J. Heller, Proceedings of the National Academy of Sciences **116**, 18316 (2019).
- [40] P. Moon and M. Koshino, Physical Review B **87**, 205404 (2013).
- [41] N. Rana, M. Mrudul, D. Kartashov, M. Ivanov, and G. Dixit, arXiv preprint arXiv:2207.10440 (2022).
- [42] N. Tancogne-Dejean, O. D. Mücke, F. X. Kärtner, and A. Rubio, Nature Communications **8**, 745 (2017).
- [43] T. Jeong, S. Jung, and K. Yee, in Conference on Lasers and Electro-Optics/Pacific Rim (Optical Society of America, 2015) p. 26C2.4.
- [44] H. Hubener, U. De Giovannini, and A. Rubio, Nano letters **18**, 1535 (2018).
- [45] C. Heide, T. Higuchi, H. B. Weber, and P. Hommelhoff, Physical Review Letters **121**, 207401 (2018).
- [46] N. Yoshikawa, T. Tamaya, and K. Tanaka, Science **356**, 736 (2017).
- [47] O. E. Alon, V. Averbukh, and N. Moiseyev, Physical Review Letters **80**, 3743 (1998).
- [48] Z. Y. Chen and R. Qin, Optics express **27**, 3761 (2019).
- [49] M. Mrudul and G. Dixit, Physical Review B **103**, 094308 (2021).
- [50] N. Saito, P. Xia, F. Lu, T. Kanai, J. Itatani, and N. Ishii, Optica **4**, 1333 (2017).
- [51] G. Vampa, C. R. McDonald, G. Orlando, P. B. Corkum, and T. Brabec, Physical Review B **91**, 064302 (2015).
- [52] K. Nagai, K. Uchida, N. Yoshikawa, T. Endo, Y. Miyata, and K. Tanaka, Communications Physics **3**, 1 (2020).
- [53] I. Gierz, M. Mitrano, H. Bromberger, C. Cacho, R. Chapman, E. Springate, S. Link, U. Starke, B. Sachs, M. Eckstein, T. Wehling, M. Katsnelson, A. Lichtenstein, and A. Cavalleri, Physical Review Letters **114**, 125503 (2015).
- [54] E. Pomarico, M. Mitrano, H. Bromberger, M. Sentef, A. Al-Temimy, C. Coletti, A. Stöhr, S. Link, U. Starke, C. Cacho, et al., Physical Review B **95**, 024304 (2017).